Prediction of Residual Stresses by Radial Basis Neural Network in HSLA-65 Steel Weldments

M. Heidari*
Department of Mechanical Engineering,
Aligudarz Branch, Islamic Azad University, Aligudarz, Iran
E-mail: moh104337@yahoo.com
*Corresponding author

Received: 13 December 2014, Revised: 7 April 2015, Accepted: 20 April 2015

Abstract: This paper investigates the residual stress fields in the vicinity of weld bead in HSLA-65 steel weldments using a neural network. This study consists of two cases: (i) the experimental analysis was carried out on the measurement of residual stresses by XRD technique. Many different specimens that were subjected to different conditions were studied. The values and distributions of residual stresses occurring in welding of HSLA-65 plate under various conditions were determined. (ii) The mathematical modeling analysis has proposed the use of radial basis (RB) NN to determine the residual stresses based on the welding conditions. The input of RBNN are welding current, welding voltage, welding heat input, travel speed of welding, wire feed speed and distance from weld. The best fitting training data set was obtained with 18 neurons in the hidden layer, which made it possible to predict residual stresses with accuracy of at least as good as the experimental error, over the whole experimental range. After training, it was found that the regression values (R^2) are 0.999664 and 0.999322 for newrbe and newrb functions respectively. Similarly, these values for testing data are 0.999425 and 0.998505, respectively. Based on the verification errors, it was shown that the radial basis function of neural network with newrbe function is superior in this particular case, and has the average error of 7.70% in predicting the residual stresses in HSLA-65. This method is conceptually straightforward, and it is also applicable to other type of welding for practical purposes.

Keywords: Artificial Neural Network, HSLA-6, Residual Stress, Radial Basis Function

Reference: Heidari, M., "Prediction of Residual Stresses by Radial Basis Neural Network in HSLA-65 Steel Weldments", Int J of Advanced Design and Manufacturing Technology, Vol. 8/ No. 2, 2015, pp. 55-64.

Biographical notes: M. Heidari received his MSc in Mechanical Engineering from Shahid Chamran University of Ahvaz in 2003. He is currently an Instructor at the Department of Mechanical Engineering, Aligudarz Branch, Islamic Azad University. His current research interest includes Residual Stresses and Fatigue life in joints of steel welding.

1 INTRODUCTION

Welding is a commonly used permanent joining process with wide applications in industries. Highly non-uniform temperature field, phase transformations and plastic deformations which occur during welding give rise to residual stress build up and distortions in the final product. The complex metallurgical processes in welding produce both tensile and compressive residual stress in different zones of the welded structure. The formation of tensile residual stress may result in initiation of fatigue cracks, stress corrosion cracking, or other types of failures.

It is important, therefore, to understand the distribution of residual stress inside and near the weldment. Ship structures are subject to a complex dynamic condition during service that are superimposed on residual stress present as a result of fit up during fabrication. In order to meet the requirement for a good combination of high strength and low-temperature fracture toughness, high-yield-strength steels (HY series) and high-strength, low-alloy steels (HSLA series) have been under development by the Navy for the last 50 years. Among them, HY-100 and HSLA-100, are used extensively in surface ship and submarine construction today, and they will continue to be the principal structural materials in the foreseeable future [1-3]. HSLA-65 plate steels can be produced using one of five plate manufacturing techniques: normalizing, controlled rolling (CR), controlled rolling followed by accelerating cooling (CR-AC), direct quenching and tempering (DQT), or conventional quenching and tempering (Q&T). The HSLA-65 steels are characterized by low carbon content and low alloy content, and they exhibit a low carbon equivalent that allows improved plate weldability. These steel processing routes ensure (a) provide the steel plate with a refined microstructure that ensures high strength and toughness; (b) eliminate or substantially reduce the need for preheating during welding; (c) resist susceptibility to hydrogen-assisted cracking (HAC) in the weld heat affected zone (HAZ) when fusion (arc) welded using low heat-input conditions; and (d) depending on section thickness, facilitate welding with heat-input up to 2 kJ/mm without significant loss of strength or toughness in the HAZ.

Such differences in processing and properties of HSLA-65 plate steels could potentially affect the selection and control of various secondary fabrication practices, including friction stir welding [4]. Barnes et al. [5, 6] produced a set of single pass full penetration friction stir bead-on-plate and butt welds in HSLA-65 steel using a range of traverse speeds (50 to 500 mm/min) and two tool materials (W-Re and PCBN). Part I describes the influence of process and tool parameters on the microstructure in the weld region. Part II is focused on the influence of these parameters on residual stress, but the presence of retained austenite evident in the diffraction pattern and X-ray tomographic investigations of tool material depositions are also discussed.

The residual stress measurements were made using white beam synchrotron X-ray diffraction (SXRD). The residual stresses were affected by the traverse speed as well as the weld tool material. While the peak residual stress at the tool shoulders remained largely unchanged (approximately equal to the nominal yield stress (450 MPa)) irrespective of weld speed or tool type, for the W-Re welds, the width of the tensile section of the residual stress profile decreased with increasing traverse speed (thus decreasing line energy). The effect of increasing traverse speed on the width of the tension zone was much less pronounced for the PCBN tool material.

Wei and Nelson examined the influence of heat input on post weld microstructure and mechanical properties of friction stir welded HSLA-65 steel [7]. To understand and model the thermos-mechanical response of HSLA-65, uniaxial compression tests were performed on cylindrical samples, using an Instron servo hydraulic testing machine and UCSD's enhanced Hopkinson technique [8]. HSLA-100 steel is a low carbon, copper precipitation strengthened steel used for surface combatant structures and non pressure hull structural ship applications as a replacement for HY-100 steel. Although there have been a number of studies of HSLA-100 steel plate and its weldments with the last 10 years [9, 10]. These investigations have been mainly centered on the microstructure properties relationship. Only a few results are available concerning the residual stress distribution in the weldment [11].

Ahmadzadeh et al. [12] presented the development of a back propagation neural network model for the prediction of maximum residual stresses produced in gas metal arc welding process. The thickness of the plate, electrode size, welding speed and current/voltage intensity have been considered as the input parameters and the maximum residual stresses due to welding as output parameters in the development of the model. The Levenberg–Marquardt method as a feedforward back propagation method has been used in this investigation. The neural network predictions have been compared with the finite element results for accuracy, and the comparison showed that the results obtained from neural network model were sufficiently accurate in predicting the residual stresses. The prediction of welding residual stresses has been the subject of investigations by several researchers using different approaches.

Finite element analysis (FEA) has been employed by most authors [13–19] for welding simulations and to predict residual stresses in different types of welded joints and materials. Xu et al. [20] used the FEM to predict the residual stresses in a tube to tube sheet weld. The effect of heat input, preheating temperature, and the gap between tube and the tube hole on residual stresses was also investigated by numerical simulation. The peak Von Mises residual stress occurred in the base metal near the interface between surface welding layer and base metal. The heat input had little effect on the residual stresses. The maximum residual stress was determined by the yield strength rather than heat input. With the preheating temperature increasing, the peak hoop stresses were decreased. With the gap between tube and the tube hole increasing, the residual stresses were increased.

Prediction of axial and hoop residual stresses in high strength carbon steel pipe weld was made by employing a sequentially coupled 3-D thermal, metallurgical and mechanical FE model [21]. In the FE model, temperature-dependent thermo-physical and mechanical properties were considered, and phase transformation plasticity were also taken into account. The results showed the importance of incorporating solid-state phase transformation in the simulation of the pipe welding. The residual stresses around a high strength quenched and tempered steel T-butt web to curved plate weld have been measured using neutron diffraction strain scanning. The results showed that the residual stresses near the weld were dominated by the welding residual stresses, while the stresses further from the weld were dominated by the bending residual stresses. The results suggest that the combination of welding-induced residual stress and significant pre-welding residual stress, as in the case of a thick bent section of plate can significantly alter the residual stress profile from that in a flat plate [22].

Brown et al. [23] presented results of the work on a series of rectangular repair welds in P275 and S690 (EN 10025) steels to validate the numerical modelling techniques used in the determination of the residual stresses generated during the repair process. The repair welds were modelled using the finite element method to make predictions of the as-welded residual stress distributions. Comparisons between the measurements and the finite element predictions generally showed good agreement, thus providing confidence in the method. Bae et al. [24] used three data-based models, support vector regression (SVR), fuzzy neural network (FNN), and their combined (FNN + SVR) models to predict the residual stress for dissimilar metal welding under a variety of welding conditions. By using a subtractive clustering (SC) method, informative data that demonstrate the characteristic behavior of the system selected to train the models from the numerical data obtained from finite element analysis under a range of welding conditions. The FNN model was optimized using a genetic algorithm. The statistical and analytical uncertainty analysis methods of the models were applied, and their uncertainties were evaluated using 60 sampled training and optimization datasets, as well as a fixed test data set. The distribution of the residual stress in the weld joint of HQ130 grade high strength steel has been investigated by means of finite element method (FEM) using ANSYS software [25]. Welding was carried out using gas shielded arc welding with a heat input of 16 KJ/cm. The results show that the stress gradient near the fusion zone is higher than any other location in the surrounding area. Unfortunately, residual stresses in HSLA-65 weldments have not been addressed well in the literature.

This paper investigates the residual stress fields in the vicinity of weld bead in HSLA-65 steel weldments using a neural network. This study consists of two parts. First, the experimental analysis was carried out on the measurement of residual stresses by XRD technique. The values and distribution of residual stresses occurring in welding of HSLA-65 plate under various conditions were determined. Next, the mathematical modeling analysis was carried out which has proposed the use of radial basis neural network to determine the residual stresses based on the welding conditions.

2 EXPERIMENTAL PROCEDURES

HSLA-65 steel is a low alloy steel, containing small amounts of alloying elements Cr, Mo, Si, Mn and Ni. The specified value of tensile strength of this steel is 1000 MPa and this steel exhibits correspondingly high hardenability. The chemical composition of the HSLA-65 steel plate used in the welding trials is summarized in Table 1, and the welding parameters are shown in Table 2. The microstructure of HSLA-65 steel contains low carbon, tempered martensite and has a wide range of properties after heat treatment. The width of the weld plate is 250 mm and the thickness is 25.4 mm. Flux cored arc welding (FCAW) is used to deposit the weld bead on the top surface of the specimen plates. Within the FCAW welded specimens, plates are welded with either high or low heat inputs with MIL-101TM welding consumable. The 0.045 in. (1.2 mm) Outershield® 91K2H (AWS: E91T1-K2M H8) provided by The Lincoln Electric Co. Welding parameters are as follows: voltage 20-32 V, current 130–305A, travel speed 5.1-9.33 mm/s, and wire feed speed 73.3-265 mm/s. Ar+25% $Co_2$is the recommended shielding gas for this consumable; however, in order to minimize the hydrogen loss, pure Argon at a flow rate of 45 ft^3/h (21.2 *L/min*) is used instead. The schematic

diagram of the weld sample is shown in Fig. 1 (h is the thickness of the test plate and l is the width). The X-ray diffraction (XRD) is the most accurate and best developed method of quantifying the residual stresses produced by some processes such as welding. XRD offers a number of advantages when compared to various mechanical methods or the nonlinear elastic ultrasonic or magnetic methods currently available. XRD is a linear–elastic method in which the residual stress in the material is calculated from the strain measured in the crystal lattice. XRD methods are not significantly influenced by material properties such as hardness, and degree of cold work. XRD is capable of high spatial resolution, approximately millimeters and depth resolution about microns, and can be applied to a wide variety of sample geometries. Vanadium-filtered CrK_α radiation of wavelength 2.290920A° is diffracted from the (211) planes of iron at $2\theta = 156^\circ$. The $\sin^2\psi$ method is used to determine residual stress. Seven ψ-angles $(0^\circ, \pm 15^\circ, \pm 30^\circ, \pm 45^\circ)$ are used. All measurements are made with a 2 mm diameter round collimator. A measurement time of 15 min is found to produce acceptable counting statistics of ± 15 Mpa. At each location, stress measurements are made in the $\phi = 0^\circ, 45^\circ$ and 90° orientations where $\phi = 0^\circ$ is defined as a direction perpendicular to the weld (transverse) and $\phi = 90^\circ$ is a direction parallel to the weld line [26].

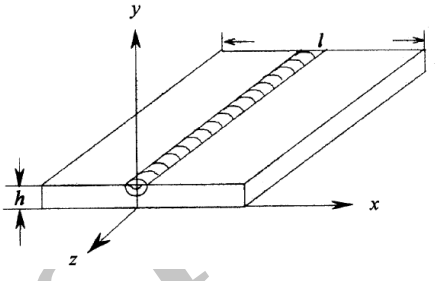

Fig. 1 Schematic diagram of the welding test plate

Table 1 Chemical composition and mechanical properties of HSLA-65 steel

Chemical composition (wt.%)											
C	V	Cu	Si	Mn	Mo	Cr	Ni	Ti	S	P	Nb
0.074	0.058	0.25	0.24	1.35	0.06	0.14	0.34	0.012	0.006	0.011	0.018

Table 2 Welding parameters used in the test

No.	Welding current (A)	Welding voltage (V)	Traveling speed mm/min	Welding heat input (Kj/mm)	Wire feed speed (mm/s)
1	130	20	306	0.4	73.3
2	130	22	408	0.37	73.3
3	180	23	490	0.8	116.6
4	180	25	350	0.7	116.6
5	220	25	420	0.8	158.3
6	220	27	560	0.5	158.3
7	265	27	315	1.2	208.33
8	265	29	330	1.3	208.33
9	305	30	390	1.3	265
10	305	32	372	1.4	265

3 ARTIFICAL NEURAL NETWORKS

Artificial NNs are non-linear mapping systems with a structure loosely based on principles observed in biological nervous systems. In greatly simplified terms as can be seen from Figure 2-a, a typical real neuron has a branching dendritic tree that collects signals from many other neurons in a limited area; a cell body that integrates collected signals and generates a response signal (as well as managing metabolic functions); and a long branching axon that distributes the response through contacts with dendritic trees of many other neurons. The response of each neuron is a relatively simple non-linear function of its inputs and is largely determined by the strengths of the connections from its inputs. In spite of the relative simplicity of the individual units, systems containing many neurons can generate complex and interesting behaviors. An ANN shown in Figure 3 is very loosely based on these ideas. In the most general terms, a NN consists of a large number of simple processors linked by weighted connections [27].

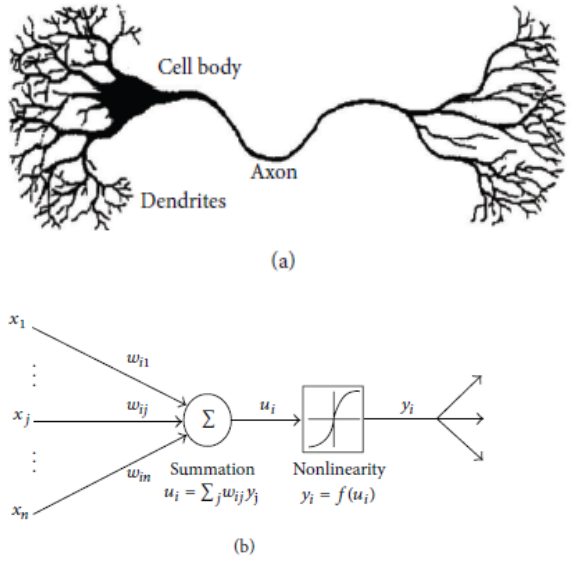

Fig. 2 (a) A biological nervous system, and (b) an artificial neuron model

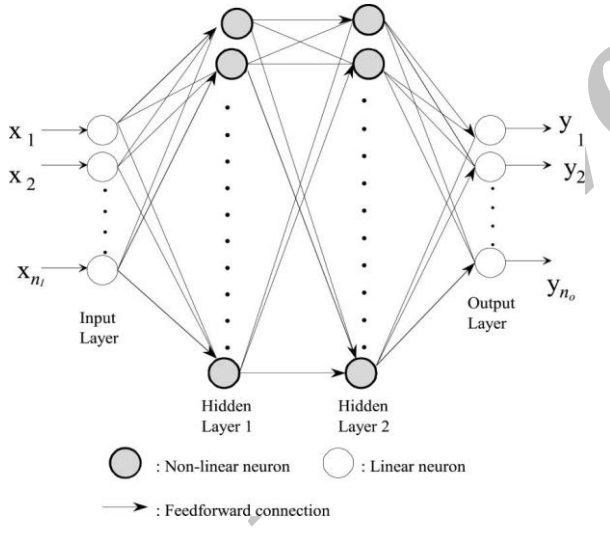

Fig. 3 A layered feed-forward artificial NN

By analogy, the processing nodes may be called neurons. Each node output depends only on information that is locally available at the node, either stored internally or arriving via the weighted connections. Each unit receives inputs from many other nodes and transmits its output to yet other nodes. By itself, a single processing element is not very powerful; it generates a scalar output with a single numerical value, which is a simple non-linear function of its inputs. The power of the system emerges from the combination of many units in an appropriate way. A network is specialized to implement different functions by varying the connection topology and the values of the connecting weights. Complex functions can be implemented by connecting units together with appropriate weights [28]. In fact, it has been shown that a sufficiently large network with an appropriate structure and property chosen weights can approximate with arbitrary accuracy any function satisfying certain broad constraints. Usually, the processing units have responses like (see Figure 2-b)

$$y = f(\sum_i u_i) \tag{1}$$

Where u_i are the output signals of hidden layer to output layer, $f(\bullet)$ is a simple non-linear function such as the sigmoid, or logistic function. This unit computes a weighted linear combination of its inputs and passes this through the non-linearity to produce a scalar output. In general, it is a bounded non-decreasing non-linear function; the logistic function is a common choice. This model is, of course, a drastically simplified approximation of real nervous systems. The intent is to capture the major characteristics important in the information processing functions of real networks without varying too much about physical constraints imposed by biology.

4 RADIAL BASIS NEURAL NETWORK

The basic concept underlying the RBNN is that of a fixed non-linear mapping of the input space to a higher dimensional space followed by a linear, adjustable output mapping. As can be shown in Figures 3 and 4, the structure of the RBNN is a model of three-layer feed forward network. The hidden layer consists of a set of basis function units, each of which has associated with its parametric vector known as receptive field. These units compute the distance between the center of the field and the input vector. The output of the units is then a function of the distance measure [29]. The RBNN is expressed by

$$f(x) = \sum_{j=1}^{N} w_j y_j (x - c_j) \tag{2}$$

Where x is a n-dimensional input vector; N, the number of hidden units and c_j, is the receptive field. The basis function is such that y_j has a significant result only in the neighborhood of c_j. There are several possibilities for the choice of basis functions. However, Gaussian type functions offer desirable properties, making the hidden units responsive to locally tuned regions. The typical examples of basis function have been explained [30]. Gaussian type activation is employed in the

proposed NN. The Gaussian activation function can be expressed as follows:

$$y_j(x) = \exp[-\frac{(x-\xi_j)^2}{(\sigma_j)^2}] \quad (3)$$

Where ξ_j is the vector representing the function center and σ is parameter affecting the spread of the radius. The chosen basis function influences both the learning and modelling abilities of the network, and will also influence the choice of learning rule used to train the network. The performance of the radial basis NN depends critically on the placement of the centres of the receptive; and the localization associated with each radial basis function (RBF) is a vital factor for attaining faster training speeds. In this study, radial basis Gaussian function and back propagation learning algorithm are employed to train the proposed NN. The learning algorithm topology, which was employed for the NN updating the weight, can define the error function as:

$$J = \frac{1}{2}\sum_{i=1}^{n_o}(y_{di}(t) - y_i(t))^2 \quad (4)$$

Where $y_{di}(t)$ are the *i*th desired outputs and $y_i(t)$ are the *i*th outputs of the network. This error function is to be minimized with respect to all the unknown parameters Θ. In the steepest descent approach the parameter vector $\Theta = [\theta_1, \theta_2, ... \theta_n]^T$ is adjusted using the increment vector $[\Delta\theta_1, \Delta\theta_2, ..., \Delta\theta_n]^T$ defined along the negative gradient direction of *J*

$$\Delta\theta_i = -\eta\frac{\partial J}{\partial \theta_i} \quad (5)$$

Although the one-hidden-layer model is used in the present application, it is useful to derive the gradient of *J* for the general case, and the result for the one-hidden-layer model can readily be obtained as a special case. Starting from the output layer *m* of the network and setting $\theta_i = W^m{}_{ij}$, the application of the chain rule gives rise to

$$\frac{\partial J}{\partial W_{ij}^m} = \frac{\partial J}{\partial y_i}\frac{\partial y_i}{\partial W_{ij}^m} \quad (6)$$

From Eq. (4)

$$\frac{\partial J}{\partial y_i} = -(y_{di} - y_i) = -\delta_i^m \quad (7)$$

Where δ_i^m is called the error signal of the *i*th neuron in the *m*th layer. From Eq. (6)

$$\frac{\partial y_i}{\partial W_{ij}^m} = x_j^{m-1} \quad (8)$$

Thus,

$$\frac{\partial J}{\partial W_{ij}^m} = -\delta_i^m x_j^{m-1} \quad (9)$$

Next, consider the *(m-1)*th layer. Using the chain rule yields:

$$\frac{\partial J}{\partial W_{ij}^{m-1}} = \sum_{k=1}^{n_o}\frac{\partial J}{\partial y_k}\frac{\partial y_k}{\partial x_i^{m-1}}\frac{\partial x_i^{m-1}}{\partial z_i^{m-1}}\frac{\partial z_i^{m-1}}{\partial W_{ij}^{m-1}} \quad (10)$$

Then

$$\frac{\partial x_i^{m-1}}{\partial z_i^{m-1}} = g'(z_i^{m-1}) \quad (11)$$

and

$$\frac{\partial z_i^{m-1}}{\partial W_{ij}^{m-1}} = x_j^{m-2} \quad (12)$$

$$g'(z) = \frac{\partial g(z)}{\partial z} \quad (13)$$

and $g(z_i)$ is the activation of neuron *i*. By defining the error signal for the *i*th neuron of the *(m-1)*th layer as:

$$\delta_i^{m-1} = g'(z_i^{m-1})\sum_{k=1}^{n_o}\delta_k^m W_{ki}^m \quad (14)$$

Eq. (4) can be rewritten as:

$$\frac{\partial J}{\partial W_{ij}^{m-1}} = -\delta_i^{m-1}x_j^{m-2} \quad (15)$$

Similarly, it can be shown that

$$\frac{\partial J}{\partial b_i^{m-1}} = -\delta_i^{m-1} \quad (16)$$

Where b_i^{m-1} is the bias input to neuron *i* in layer *(m-1)*. By carrying on this procedure, Eqs. (14)–(16) can be used as a general algorithm for updating weights in other layers. Eqs. (14)–(16) indicate how the error signals propagate backwards from the output layer of the network through the hidden layer to the input layer, hence the name back propagation. The steepest-descent minimization of the error function defined in Eq. (4) produces the following increments for updating Θ:

$$\Delta W_{ij}^m(t) = \eta_w\delta_i^m(t)x_j^{m-1}(t) \quad (17)$$

$$\Delta b_i^m(t) = \eta_b\delta_i^m(t) \quad (18)$$

Where in the output layer

$$\delta_i^m(t) = y_{di}(t) - y_i(t) \tag{19}$$

and in other layers

$$\delta_i^m(t) = g'(z_i^m(t)) \sum_j \delta_j^{m+1}(t) W_{ji}^{m+1}(t-1) \tag{20}$$

The constants $\eta_w\,(0<\eta_w<1)$ and $\eta_b\,(0<\eta_b<1)$ represent the learning rates for the weights and biases respectively [31]. In practice, a large value of the learning rate would be preferable, because this would result in rapid learning. Unfortunately, a large value of the learning rate can also lead to oscillation or even divergence. To help speed up learning, but avoid undue oscillations, a momentum term is usually included so that Eqs. (17) and (18) become:

$$\Delta W_{ij}^m(t) = \eta_w \delta_i^m(t) x_j^{m-1}(t) + \mu_w \Delta W_{ij}^m(t-1) \tag{21}$$

$$\Delta b_i^m(t) = \eta_b \delta_i^m(t) + \mu_b \Delta b_i^m(t-1) \tag{22}$$

Where η_w and η_b are momentum constants, which determine the effect of past changes of $\Delta W_{ij}^m(t)$ and $\Delta b_i^m(t)$ on the current updating direction in the weight and the bias space respectively. This effectively filters out high frequency variations in the error surface. To summarize, the back propagation algorithm updates the weights and thresholds of the networks according to:

$$W_{ij}^m(t) = W_{ij}^m(t-1) + \Delta W_{ij}^m(t) \tag{23}$$

and

$$b_i^m(t) = b_i^m(t-1) + \Delta b_i^m(t) \tag{24}$$

Where the increments $\Delta W_{ij}^m(t)$ and $\Delta b_i^m(t)$ are given in Eqs. (21) and (22).

5 RESULTS AND DISCUSSION

A simulation study was carried out using radial basis Gaussian NN for the estimation residual stress of a FCAW HSLA-65 steel. The NN predictors for the residual stress of HSLA-65, has been shown in Figure 4. The back propagation algorithm was used to update the network weights. Training parameters of the network are given in Table 3.

The nodes in the input and output layer are determined by the number of predictors and predicted variables. In this research there are 6 nodes in the input layers due to the number of input variables, and 3 nodes in the output layer, for similar reasons. The RBNN itself consists of a single hidden layer with a RBF and a linear output layer. The hidden layer has 18 non-linear neurons. Modeling of residual stresses with RBF neural networks is composed of two stages: training and testing of the networks with experimental data. Total 80 such data sets were used, of which 70 were selected randomly and used for training purposes, whilst the remaining 10 data sets were presented to the trained networks as new application data for verification (testing) purposes. Thus, the networks were evaluated using data that had not been used for training.

Table 3 Training parameters of the RBNN

Network	η	μ	n_I	n_H	n_o	N	AF
RBNN	0.001	0.01	6	18	3	2639	GF

η: learning rate; μ: momentum term; n_I: number of input units; n_H: number of hidden units; n_o: number of output units; N: training numbers; AF: activation function; GF: Gaussian function.

Before the ANN could be trained and the mapping learnt, it is important to process the experimental data into patterns. For the training of the network the Matlab Neural Network Toolbox is used [32]. Two functions, namely newrbe and newrb have been used for creating of RBF networks. The stopping criteria are adjusted, that the mean square error should be less than 0.01 and the number of epochs (iterations) should be less than 50000. Spread factor (S) value of Gaussian activation functions in the hidden layer is the parameter that should be determined by trial and error when using MATLAB neural network toolbox for designing RBF networks.

Table 4 The effects of different number of hidden neurons on the RBF network performance (S=4)

No. of hidden neurons	Training error (MSE)	Average error in predicting TRS (%)	Average error in predicting LRS (%)	Average error in predicting DRS (%)	Total average error (%)
12	0.0151	16.87	7.35	12.1	12.16
14	0.014	9.66	6.77	8.23	8.22
16	0.0131	13.43	9.02	11.54	11.33
18	0.0115	8.95	8.15	6	7.70
20	0.0113	11.72	7.73	9.68	9.71
22	0.0107	12.02	8.48	10.25	10.25

In the present case, it was found by trial and error that 18 hidden neurons with the spread factor of 4, can give a model, which has the best performance in the verification stage [33]. Table 4 shows the effect of the number of hidden neurons on the RBF network performance. A stress profile along the $\phi = 45^\circ$ direction from the weld bead is also shown as well as

general profiles for both the transverse $(\phi = 0^\circ)$ and the longitudinal $(\phi = 90^\circ)$ residual stresses. The results of surface residual stress measurements with XRD and RBNN have been shown in Figures 5 and 6. As shown in Figures 5 and 6, the results of newrbe and newrb function of RBNN have been shown in the transverse direction of the bead weld. These stress profiles are for condition number 7 and 10 in Table 3, respectively.

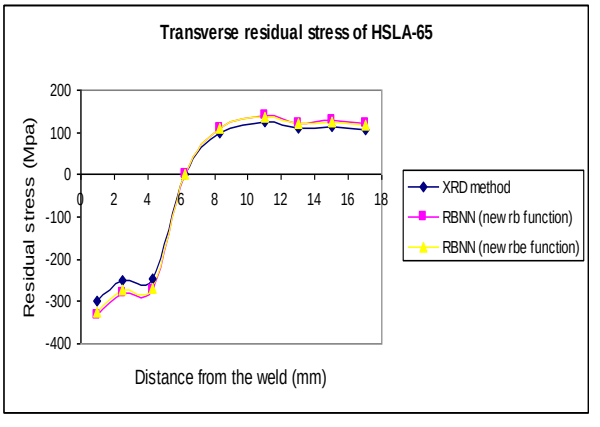

Fig. 5 Transverse residual stress distributions for condition No. 7 $(\phi = 0^\circ)$

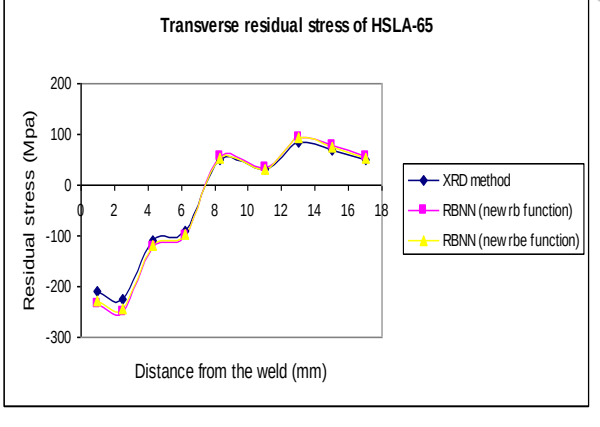

Fig. 6 Transverse residual stress distributions for condition No. 10 $(\phi = 0^\circ)$

Figures 7, 8, 9 and 10 show the residual stress profiles for longitudinal and $\phi = 45^\circ$ at the same pervious condition numbers. Tensile stress states in the longitudinal direction in the residual stress (condition No. 7, 10) are shown in Figures 7 and 8. This tensile stress is a result of shrinkage of highly heated areas near weld zone being restrained by the surrounding colder zone during the rapid heating and subsequent cooling in welding. The longitudinal stress at condition No. 7 reaches a maximum of approximately 200 MPa, 2.5 mm from the weld bead, then gradually decreases to a constant tensile stress of about 40~50 MPa. The transverse residual stress profiles show a considerable gradient as a function of distance from the weld edge line. The stress near the weld zone is highly compressive, reaching a level of approximately -300 MPa at condition No. 7. Then the stress state changes to tensile at 7.3 mm away from the weld edge line and reaches a constant value of 100~150 MPa. The compressive stress may be attributed partly to the effect of phase transformation in steel, since the volume expansion associated with the austenite to martensite/bainite phases may increase the compressive stress level.

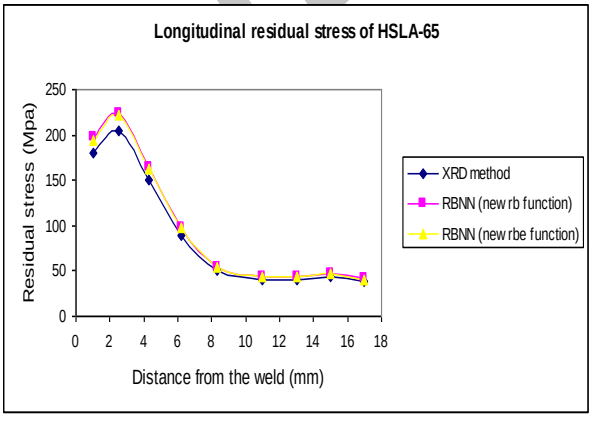

Fig. 7 Longitudinal residual stress distributions for condition No. 7 $(\phi = 90^\circ)$

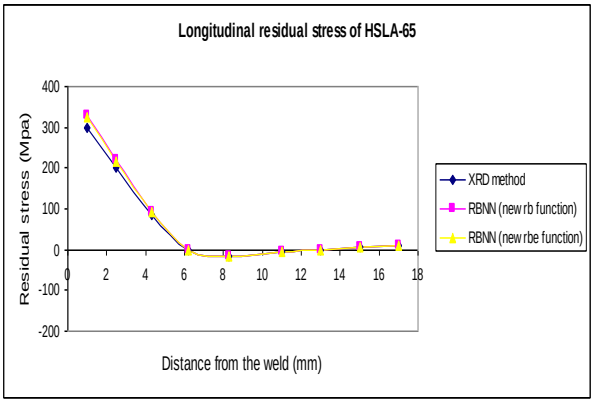

Fig. 8 Longitudinal residual stress distributions for condition No. 10 $(\phi = 90^\circ)$

The residual stress profiles at the surface of the sample are shown in Figures 6, 8 and 10 at condition No. 10. It is apparent that the residual stress shape is qualitatively similar to that of the sample at condition No. 7. The

magnitudes are, however, somewhat different from each other. The residual stress of this condition has generally a smaller absolute value because a higher welding heat input was adopted. This result demonstrates clearly that welding heat input has a significant effect on the surface residual stress state.

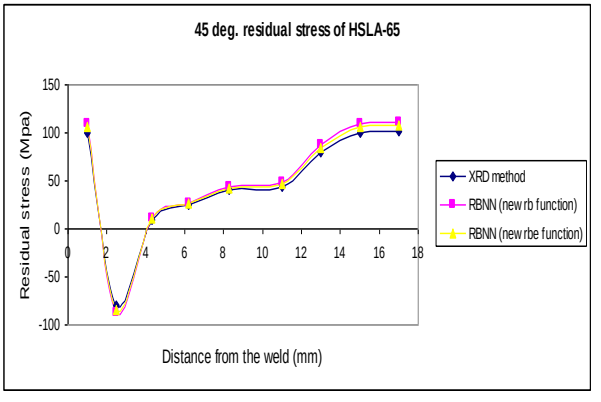

Fig. 9 Residual stress distributions for condition No. 7 ($\phi = 45^\circ$)

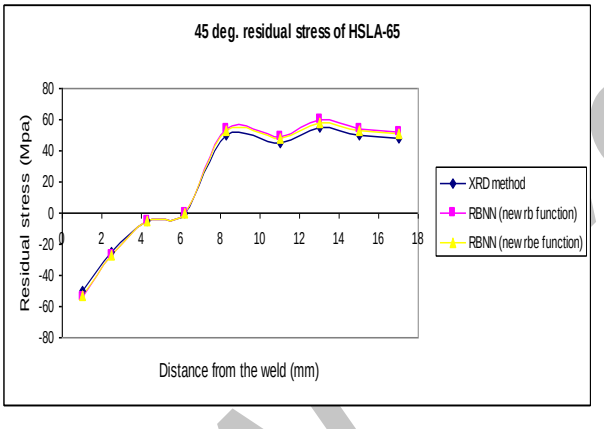

Fig. 10 Residual stress distributions for condition No. 10 ($\phi = 45^\circ$)

6 CONCLUSION

In this paper, two supervised neural networks have been used for Flux-Cored Arc Welding of HSLA-65. An effort was made to include as many different FCAW conditions as possible that influence the process. A number of observations may be drawn from this study.

1. The simulation results show the advantages of the radial basis Gaussian network in the fast convergence of the results of different approaches.
2. The results show that, estimation by newrbe function is better than newrb function because it has less error than other functions and the regression value is 0.999664.
3. Transverse residual stresses ($\phi = 0^\circ$) are always compressive on the surface near the weld, and gradually become tensile as the distance from the weld increases. Longitudinal residual stress ($\phi = 90^\circ$) is usually tensile on the surface near the weld, and slowly decreases as the distance from the weld increases. The residual stress profiles of $\phi = 45^\circ$ direction from the weld are always between the profiles of the longitudinal stress and transverse stress.
4. Specimens which are subjected to different welding heat input have similar distributions of residual stress on the surface, but the magnitudes of stresses are different. Higher welding heat input generates smaller stress.
5. The results show that increasing the welding speed reduces the reaction time for weld, as an external acting force. The result of lack of enough reaction time is a reduction in the magnitude of residual stresses.

REFERENCES

[1] Montemarano, T. W., Sack, B. P., Gudas, J. P., Vassilaros, M. G., and Vanderveldt, H. H., "High Strength Low Alloy Steels in Naval Construction", Journal of Ship Production, Vol. 2, No. 3, 1986, pp. 145–162.

[2] Czyryca, E. J., Link, R. E., Wong, R. J., Aylor, D. A., Montemarano, T. W., and Gudas, J. P., "Development and Certification of HSLA-100 Steel for Naval Ship Construction", Naval Engineers Journal, Vol. 102, No. 3, 1990, pp. 63–82.

[3] DeLoach, J. J., Null, C., Flore, S., and Konkol, P., "The Right Welding Wire Could Help the U.S. Navy Save Millions", Welding Journal, Vol. 78, No.6, 1999, pp. 55–58.

[4] Sampath, K., "An Understanding of HSLA-65 Plate Steels", Journal of Materials Engineering and Performance, Vol. 15, No. 1, 2006, pp. 32-40.

[5] Barnes, S. J., Bhatti, A. R., Steuwer, A., Johnson, R., Altenkirch, J., and Withers, P. J., "Friction Stir Welding in HSLA-65 Steel: Part I. Influence of Weld Speed and Tool Material on Microstructural Development", Metallurgical and Materials Transactions A., Vol. 43, No.7, 2012, pp. 2342-2355.

[6] Steuwer, A., Barnes, S. J., Altenkirch, J., Johnson, R., and Withers P. J., "Friction Stir Welding of HSLA-65 Steel: Part II. The Influence of Weld Speed and Tool Material on the Residual Stress Distribution and Tool Wear", Metallurgical and Materials Transactions A, Vol. 43, No.7, 2012, pp. 2356-2365.

[7] Wei, L., Nelson, T. W., "Influence of Heat Input on Post Weld Microstructure and Mechanical Properties of Friction Stir Welded HSLA-65 Steel",

Materials Science and Engineering: A. Vol. 556, 2012, pp. 51–59.

[8] Nasser, S. N., Guo, W. G., "Thermo Mechanical Response of HSLA-65 Steel Plates: Experiments and Modeling", Mechanics of Materials. Vol. 37, No. 2, 2005, pp. 379–405.

[9] Czyryca, E. J., Link, R. E., and Wong, R. J., "Evaluation of HSLA-100 Steel for Surface Combatant Structural Certification", DTRC/SME-89/15, Bethesda, Maryland, 1989, pp. 1.

[10] Spanos, G., Fonda, R. W., Vandermeer, R. A., and Matuszski, A., "Microstrucral Change in HSLA-100 Steel Thermally Cycled Simulate the Heat–Affected Zone During Welding", Metallurgical and Materials Transactions, Vol. 26, No.12, 1995, pp. 3277-3293.

[11] Blackburn, J. M. "An Overview of Some Current Research on the Welding Residual Stresses and Distortion in the U.S. Navy", 1996, IIW Doc. X-1359-96.

[12] Ahmadzadeh, M., Hoseinifard, A., Saranjam, B., and Salimi, H. R., "Prediction of Residual Stresses in Gas arc Welding by Back Propagation Neural Network", NDT & E International, Vol. 52, 2012, pp. 136–143.

[13] Zhang, J., Dong, P., and Brust, F., "Residual Stress Analysis and Fracture Assessment of Weld Joints in Moment Frames ASME. PVP-Fracture", Fatigue and Weld Residual Stress, Vol. 393, 1999, pp. 201-207.

[14] Preston, R., Smith, S., Shercliff, H.,and Withers, P., "An Investigation in to the Residual Stresses in Aanaluminum 2024 Test Weld", ASME. PVP—Fracture, Fatigue and Weld Residual Stress. Vol. 393, 1999, pp. 265-7.

[15] Dong, P., Hong, J., Bynum, J., and Rogers, P., "Analysis of residual stresses in Al–Li alloy repair welds", ASME, PVP—Approximate Methods Des Anal Press Vessels Pip Compon, Vol. 347, 1997, pp. 61–75.

[16] Karlsson, R. I., Josefson, B. L., "Three-Dimensional Finite Element Analysis of Temperatures and Stresses in a Single-Pass Butt-Welded Pipe", ASME J Pressure Vessel Technol, Vol. 112, 1990, pp. 76-84.

[17] Goldak, J., Chakravarti, A., and Bibby, M. A. "New Finite Element Model for Welding Heat Sources", Metall Trans B, Vol. 15B, 1984, pp. 299-305.

[18] Goldak, J., "Distortion and Residual Stress in Welds: the Next Generation", 8th Trends in Welding Research, 2009, pp. 45–52.

[19] Junek, L., Slovacek, M., Magula, V., and Ochodek, V., "Residual Stress Simulation Incorporating Weld HAZ Microstructure", ASME PVP—Fracture, Fatigue and Weld Residual Stress. Vol. 393, 1999, pp. 179-92.

[20] Xu, S., Wang, W., "Numerical Investigation on Weld Residual Stresses in Tube to Tube Sheet Joint of a Heat Exchanger", International Journal of Pressure Vessels and Piping, Vol. 101, 2013, pp. 37-44.

[21] Lee, C. H., Chang, K. H., "Prediction of Residual Stresses in High Strength Carbon Steel Pipe Weld Considering Solid-State Phase Transformation Effects", Computers & Structures, Vol. 89, 2011, pp. 256-265.

[22] Pearce, S. V., Linton, V. M., and Oliver, E. C., "Residual Stress in a Thick Section High Strength T-Butt Weld. Materials Science and Engineering: A", Vol. 480, 2008, pp. 411-418.

[23] Brown, T. B., Dauda, T. A., Truman, C. E., Smith, D. J., Memhard, D., and Pfeiffer, W., "Predictions and Measurements of Residual Stress in Repair Welds in Plates", International Journal of Pressure Vessels and Piping, Vol. 83, 2006, pp. 809-818.

[24] Bae, I. H., Lim, D. H., Gyun, M. N, and Kim, J. W., "Prediction of Residual Stress in the Welding Zone of Dissimilar Metals Using Data-Based Models and Uncertainty Analysis", Nuclear Engineering and Design, Vol. 240, 2010, pp. 2555–2564.

[25] Yajiang, L., Juan, W., Maoai, C., and Xiaoqin, S., "Finite Element Analysis of Residual Stress in the Welded Zone of a High Strength Steel", Bull. Mater. Sci., Vol. 27, No. 2, 2004, pp. 127–132.

[26] Withers, P., Turski, M., Edwards, L., Bouchard, P., and Buttle, D., "Recent Advances in Residual Stress Measurement", International Journal of Pressure Vessels and Piping, Vol. 85, No. 3, 2008, pp. 118-127.

[27] El-Kassas, E. M. A., Mackie, R. I., and El-Sheikh, A. I., "Using Neural Networks in Cold-Formed Steel Design", Computers & Structures, Vol. 79, 2001, pp. 1687-1696.

[28] Freeman, J. A., "Simulating Neural Networks", Addison–Wesley Publishing Company, Inc., New York, 1994.

[29] Wasserman, P. D., "Neural Computing: Theory and Practice", Van Nostrand Reinhold, New York, 1989.

[30] Heidari, M., Homaei, H., "Design of a PID Controller for Suspension System by Back Propagation Neural Network", Journal of Engineering, Vol. 2013, 2013, pp. 1-9.

[31] Jacobs R. A., "Increased Rates of Convergence Through Learning Rate Adaptation", Neural Network, Vol. 1, 1988, pp. 295-307.

[32] Demuth, H., Beale, M., "Matlab Neural Networks Toolbox", User's Guide. Copyright 1992-2001, The Math Works, Inc., See also URL http://www.mathworks.com.

[33] Zhang, H., Wei, W., and Mingchen, Y., "Boundedness and Convergence of Batch Back-Propagation Algorithm with Penalty for Feedforward Neural Networks", Neurocomputing, Vol. 89, 2012, pp. 141-146.